ADVANCED FUNCTIONAL MATERIALS

FULL PAPER

DOI: 10.1002/adfm.200600390

Hierarchical Shelled ZnO Structures Made of Bunched Nanowire Arrays**

By *Peng Jiang*,* *Jian-Jun Zhou*, *Hai-Feng Fang*, *Chao-Ying Wang*, *Zhong Lin Wang*,* and *Si-Shen Xie**

The size- and morphology-controlled growth of ZnO nanowire (NW) arrays is potentially of interest for the design of advanced catalysts and nanodevices. By adjusting the reaction temperature, shelled structures of ZnO made of bunched ZnO NW arrays are prepared, grown out of metallic Zn microspheres through a wet-chemical route in a closed Teflon reactor. In this process, ZnO NWs are nucleated and subsequently grown into NWs on the surfaces of the microspheres as well as in strong alkali solution under the condition of the pre-existence of zincate (ZnO_2^{2-}) ions. At a higher temperature (200 °C), three different types of bunched ZnO NW or sub-micrometer rodlike (SMR) aggregates are observed. At room temperature, however, the bunched ZnO NW arrays are found only to occur on the Zn microsphere surface, while double-pyramid-shaped or rhombus-shaped ZnO particles are formed in solution. The ZnO NWs exhibit an ultrathin structure with a length of ca. 500 nm and a diameter of ca. 10 nm. The phenomenon may be well understood by the temperature-dependent growth process involved in different nucleation sources. A growth mechanism has been proposed in which the degree of ZnO_2^{2-}saturation in the reaction solution plays a key role in controlling the nucleation and growth of the ZnO NWs or SMRs as well as in oxidizing the metallic Zn microspheres. Based on this consideration, ultrathin ZnO NW cluster arrays on the Zn microspheres are successfully obtained. Raman spectroscopy and photoluminescence measurements of the ultrathin ZnO NW cluster arrays have also been performed.

1. Introduction

The preparation of size-controlled, multidimensional (MD) composite nanomaterials is of great importance for the development of advanced catalysts and gas sensors.[1] Materials with a large surface-to-volume ratio are expected to have superior performances because of self-aggregation of the nanoscale units without surface capping. Self-assembly driven by physical or chemical interaction is an effective route to construct nanoscale materials with a MD structure.[2]

ZnO, a wide-bandgap semiconductor ($E_g = 3.37$ eV at 300 K) with a large exciton binding energy (60 meV), is a versatile, multifunctional material. It has been extensively used in several industrial products, such as ceramics, rubber additives, pigments, and medicines.[3–6] Recently, the discovery of the ultraviolet laser,[7] piezoelectric,[8] and photocatalysis properties[9] of ZnO nanostructures has triggered several new applications. Various physical and chemical routes, such as physical vapor deposition,[10] thermal evaporation,[11] chemical vapor deposition,[12] metal–organic chemical vapor deposition,[13] and colloidal wetting chemical synthesis[14–16] have been used to prepare a wide range of ZnO nanostructures, including novel ZnO nanoarchitectures such as nanoparticles,[17] -wires (NWs),[18] -belts,[19] -tubes,[20] -rings,[21] -helixes/-springs,[22] -bows,[23] -combs,[24] and -cages.[25] However, achieving control over the size and morphology of the grown ZnO nanostructures and their further self-organization into 2D or MD superstructures is still challenging. A complicated hierarchical ZnO NW structure has been obtained by thermal deposition of metallic Zn powder,[26] but by what means control over the morphology and size of the ZnO NWs on the curved surfaces of the Zn microspheres can be achieved remains an open question. In addition, the large-scale industrial preparation of MD ZnO nanomaterials by a controlled methodology is very difficult. In comparison with traditional vapor deposition approaches, wet-chemical methods can provide a better opportunity for control over the size and morphology of basic ZnO nanometer-scale units for building MD ZnO structures. More importantly, the route allows for an easier realization of the industrial process-

[*] Prof. P. Jiang, Prof. Z. L. Wang, Prof. S.-S. Xie, H.-F. Fang
National Center for Nanoscience and Technology
No. 2, 1st North Street, Zhong-Guan-Cun, Hai-Dian District
Beijing 100080 (P.R. China)
E-mail: pjiang_hlx@yahoo.com; zhong.wang@mse.gatech.edu; ssxie@aphy.iphy.ac.cn
Prof. Z.-L. Wang
School of Materials Science and Engineering
Georgia Institute of Technology
Atlanta, GA 30332-0245 (USA)
Prof. S.-S. Xie, Dr. J.-J. Zhou, C.-Y. Wang
Institute of Physics, Chinese Academy of Sciences (CAS)
Beijing 100083 (P.R. China)

[**] The work was financially supported by the Scientific Research Foundation for the Returned Overseas Chinese Scholars, State Education Ministry, the National Natural Science Foundation of China (NSFC90406024), "863" and "973" National Key Basic Research Project (2005CB724700). The Cooperation Lab of the National Center for Nanoscience and Technology also provided support.

ing of MD ZnO nanomaterials with controllable sizes and morphologies.

In the present report, we explore a simple wet-chemical route for the controlled growth of bunched ZnO NWs and self-assembled hierarchical structures under various reaction temperature conditions. The morphology, size, and structure of the ZnO NWs have been investigated. A possible mechanism has been suggested to elucidate the formation and growth of the hierarchical structures. The study shows that it is possible to achieve size control over ZnO NWs on curved surfaces of metallic Zn microspheres by controlling the reaction temperature with a simple one-step reaction in a closed reactor.

2. Results and Discussion

In the preparation process of the ZnO nanomaterials, Zn powder was added to a highly concentrated aqueous solution of sodium hydroxide containing a certain concentration of zinc nitrate. ZnO can nucleate and subsequently grow into NWs on the surface of the metallic Zn microspheres in concentrated NaOH solution in the presence of zincate (ZnO_2^{2-}) ions in a closed Teflon reactor. The size of the ZnO NWs can be easily controlled by adjusting the reaction temperature.

2.1. Morphology and Structure of Bunched ZnO NWs

The metallic Zn powder used for the preparation of the ZnO NW aggregates consisted of spherical Zn particles with an average size of several micrometers. A few larger Zn microspheres with sizes of 10–15 μm also exist in the powder, as shown in Figure 1. Zn can be converted into ZnO by reaction with a concentrated NaOH solution. Figure 2a demonstrates a typical scanning electron microscopy (SEM) image of the reaction product, obtained from a reaction performed at 200 °C. Three different types of ZnO hierarchical structures, with sizes from 10 to 15 μm, can be found. The first one has a microspheric crust structure with an open mouth and a size of ca. 14 μm. The crust is composed of short ZnO NWs with diameters of 100–500 nm and lengths in the range of 1–2 μm (see insert in Fig. 2b), which are radially oriented with their growth axes pointing towards the center of the microsphere. Obviously, the formation of these hollow microspheres with a ZnO NW shell may result from oxidation of the larger Zn microspheres by strong alkali. The second structure has a smaller void at the center of the radially self-organized ZnO sub-micrometer rodlike (SMR) bunches (see Fig. 2c). The ZnO SMRs are about 7 μm long and 700 nm wide with two spike-like ends, much longer and thicker than those

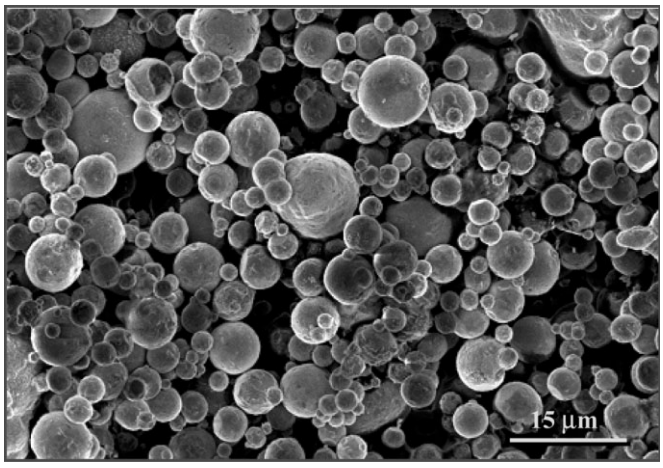

Figure 1. A representative field-effect scanning electron microscopy (FE-SEM) image of the Zn powder, which consists of metallic Zn microspheres with a diameter of several micrometers. Several larger particles with diameters of 10–15 μm are visible in the SEM image.

grown out of larger Zn microspheres. The insert in Figure 2c demonstrates the growing front of the ZnO SMRs along the [0001] direction. The SMRs are bounded by six {1010} facets. The structure may be formed by oxidation of smaller Zn microspheres followed by growth of the ZnO NWs. The third structure is similar to the second, but without a void at the center of the aggregate (see Fig. 2d). To elucidate the origin of the third structure, an experiment was performed using only ZnO_2^{2-} solution, without Zn powder, under the same conditions. Similar self-organized ZnO SMR bunches were formed, as shown in Figure 2e. Thus, the third structure type probably originated from the nucleation and growth of ZnO formed by $Zn(OH)_4^{2-}$ ion units in solution rather than from the Zn microspheres.

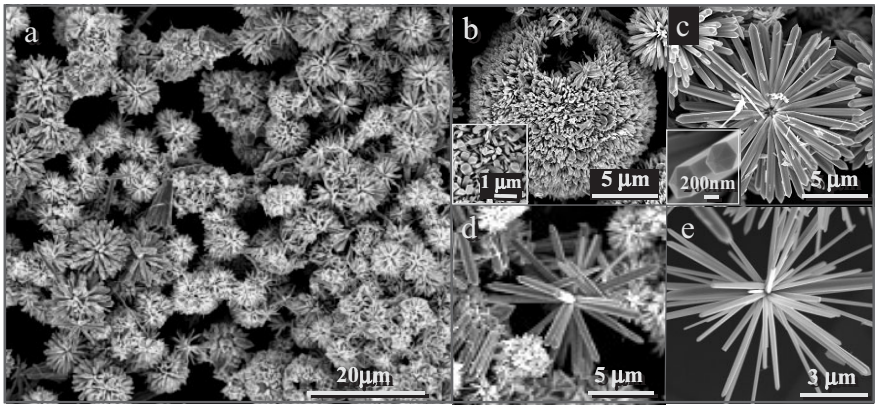

Figure 2. FE-SEM images of the multidimensional ZnO nanowires (NW) and sub-micrometer rodlike (SMR) aggregates prepared from the Zn powder in zincate ion solution at 200 °C for 2 h. a) General morphology of the product. b) Multidimensional urchinlike ZnO NW hollow microsphere; the insert shows details of the ZnO NWs. c) Multidimensional urchinlike ZnO SMR aggregate with a smaller void at the center and uniform radial ZnO SMRs; the insert shows the growth ends of the ZnO SMRs. d) Nanostructure with no void at the center. e) Multidimensional urchinlike ZnO SMR aggregate prepared from a zincate ion solution without the addition of the Zn powder.

ADVANCED FUNCTIONAL MATERIALS

To further understand the growth process of the bunched ZnO NW hierarchical structures, several adjustments in the experimental conditions were made. Figure 3 shows SEM images of products obtained at reaction temperatures of 100, 60, and 25 °C while keeping other conditions unchanged. As seen in Figure 3a–c, three different kinds of bunched ZnO NW arrays were observed after the reaction was carried out at 100 °C for 2 h. The morphologies and sizes of the ZnO NWs were very similar to those obtained at 200 °C. When the reaction was performed at 60 °C for 2 h the ZnO hierarchical structures were still produced, but the sizes of the ZnO NWs were rather small, especially those of NWs grown on the Zn microspheres (Fig. 3d and e). The thin ZnO NWs with an average diameter of several tens of nanometers self-organize to form ZnO NW bunches. The clusters are about 700 nm thick. The thickness is close to the average diameter of ZnO NWs grown from smaller Zn microspheres at 200 °C. At the same time, the diameter and length of ZnO NWs nucleated and grown in solution also decreased to ca. 300 nm and 3 μm, respectively (see Fig. 3f). At 25 °C, we extended the reaction time to 12 h. Only hollow microspheres made of self-organized NWs with open mouths were found; the ZnO NWs, which also self-organized into bunches, had an average diameter of ca. 10 nm and lengths of ca. 500 nm. No self-organized hierarchical ZnO NW structures with a small void at the center were found (see Fig. 3g and h). It is noteworthy that a large amount of rhombus-shaped ZnO particles appeared around the bunched ZnO NW hollow microspheres (see Fig. 3g–i).

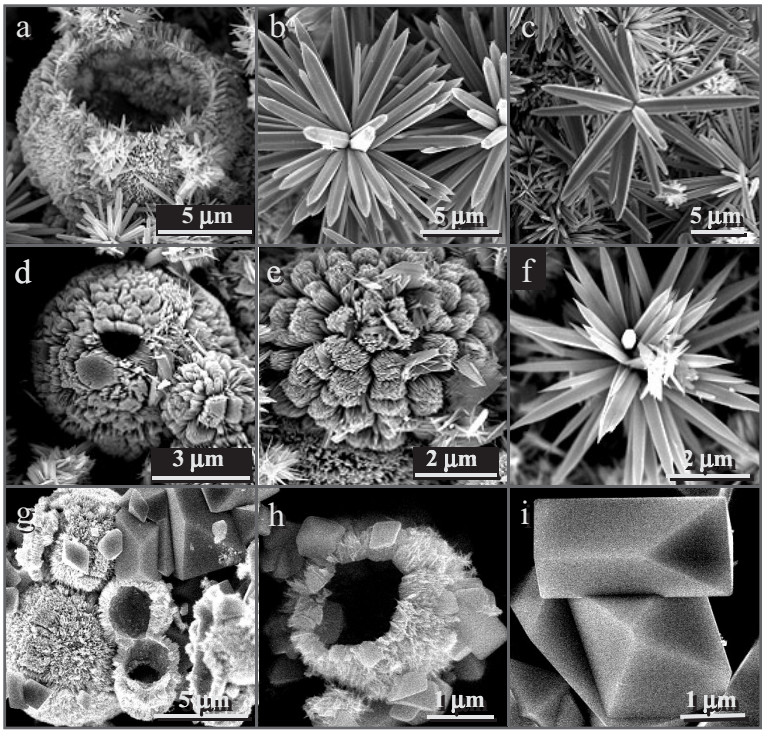

Figure 3. FE-SEM images of multidimensional ZnO NWs or SMR aggregates prepared from the Zn powder in zincate ion solution under various temperature conditions. a–c) 100 °C, 2 h. d–f) 60 °C, 2 h. g–i) 25 °C, 12 h.

The crystal structures of the ZnO NWs grown on the Zn microspheres in solution were further investigated by X-ray diffraction (XRD). Figure 4 demonstrates XRD patterns for the as-synthesized products obtained from various reaction temperature conditions. All diffraction peaks can be indexed to the pure wurtzite phase of ZnO (Joint Committee on Powder Diffraction Standards (JCPDS) Card No. 89-1397). In comparison with the standard XRD pattern for bulk ZnO, the enhanced (0002) reflections may originate from the oriented growth of the constituent NWs along the [0001] direction.

2.2. Growth Mechanism of Bunched ZnO NW Arrays in Alkali Solution

In general, the formation of ZnO crystals can be divided into two processes, that is, nucleation and growth. The nucleation of ZnO on the metallic Zn microspheres as well as in solution is the first step for the formation of the ZnO NWs. In the present case, two kinds of chemical reactions can take place in the alkali solution system, as shown below:

$$Zn + 4\,OH^- \rightarrow ZnO_2^{2-} + 2\,H_2O \quad (1)$$

$$ZnO_2^{2-} + H_2O \leftrightarrow ZnO + 2\,OH^- \quad (2)$$

This means that Zn atoms on the Zn microsphere surface are firstly converted into soluble ZnO_2^{2-} by Equation 1, and that these anions then further react with water to become solid-state ZnO by Equation 2. In fact, the real formation process of the Zn NWs is quite complicated.

Usually, surfaces of the Zn microspheres are made of many facets with a thin layer of natural oxide. In the absence of ZnO_2^{2-} ions, the oxide layer can be completely dissolved in highly concentrated NaOH solution by Equation 2, in which the chemical equilibrium tends to proceed towards the left. Afterwards, the Zn atoms on the Zn microsphere surface are in contact with OH^- ions, resulting in oxidation as given by Equation 1. Subsequently, a new oxide layer can be formed on the surface of the Zn microspheres and then dissolved in the solution by OH^- until the concentration of ZnO_2^{2-} ions in the solution reaches saturation. The two chemical reactions are beneficial to the production of ZnO_2^{2-} ions. Once the concentration of ZnO_2^{2-} ions reaches saturation, nucleation and subsequent growth of the ZnO NWs may occur on the surfaces of the Zn microspheres as well as in solution. Therefore, the degree of saturation of ZnO_2^{2-} ions in the reaction solution is a key factor for the formation of the ZnO NWs. Furthermore, the original oxide layer formed on the Zn microsphere surface in air might also play a role. To confirm this point, we employed the Zn microspheres after removing the oxide layer to interact with the ZnO_2^{2-} ion solution at 200 °C for 2 h. The result demonstrates that the nucleation and growth of the ZnO

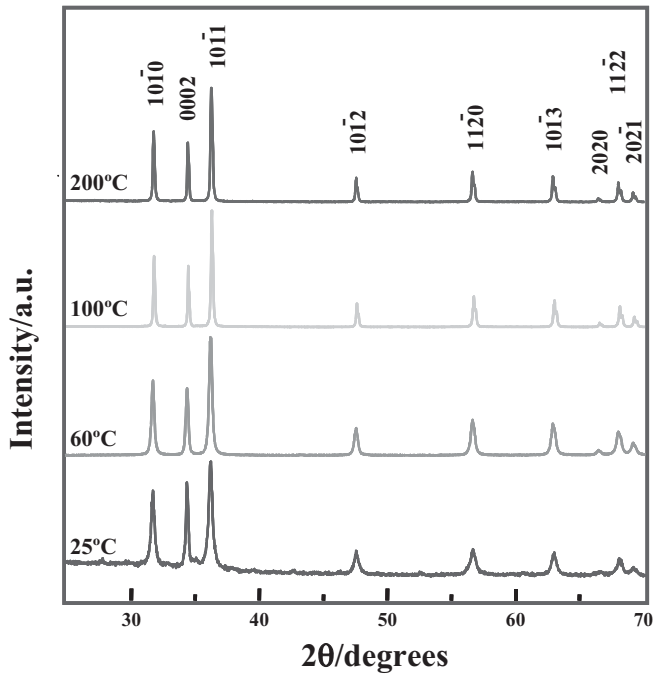

Figure 4. XRD patterns of the ZnO products prepared at various reaction temperatures. All peaks can be attributed to the pure wurtzite phase of ZnO.

happened selectively on some active sites and is determined by factors such as angle, side, and certain facets. It is worth noting that the oxidation rate of Zn is very slow, even at 200 °C (see Fig. 5 and insert).

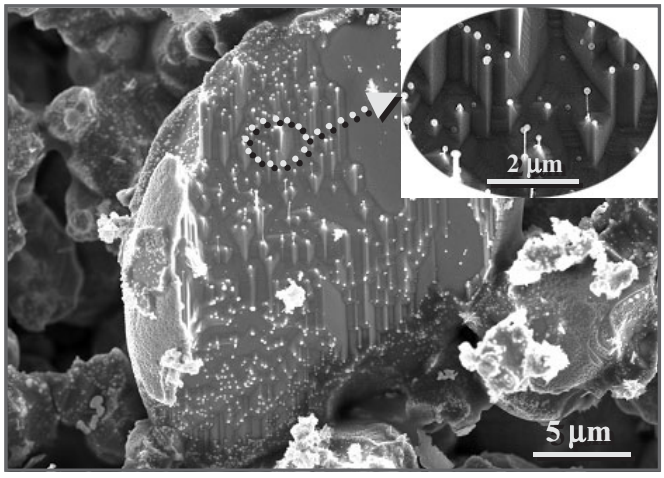

Figure 5. Typical FE-SEM images of fresh Zn microspheres without an oxide layer reacting with the zincate ion solution at 200 °C, revealing that the nucleation and growth of the ZnO NWs occurs selectively at some active sites with certain angles, sides, facets. The insert demonstrates more details.

When investigating the oxidation behavior of a Zn electrode in concentrated alkaline KOH electrolyte, Powers et al.[27–29] found that two types of ZnO could be formed on the surface of the polished Zn electrode. In the case of no convection current, type I ZnO crystals were first homogeneously nucleated in the electrolyte. After the surfaces of the Zn electrode were covered by the type I ZnO crystals, type II ZnO with bulk appearance emerged and continued to grow until all the Zn was consumed. In comparison to our case, the concentration of the ZnO_2^{2-} ions can reach its saturation value very fast because of the pre-existence of the ZnO_2^{2-} ions in the solution, and the removal rate of ZnO on the Zn microspheres by OH^- can be drastically reduced. Therefore, nucleation and growth of ZnO may occur on the surfaces of the Zn microspheres and in the solution during a short time period. On the Zn microsphere surface, the initial nucleation of the ZnO obeys a basic epitaxial orientation relationship with the base crystal facets of Zn. The large lattice mismatch between Zn and ZnO (ca. 23.7 %) leads to the formation of small ZnO islands and the occurrence of gaps or pores among the ZnO nanocrystallites due to strain induced by phase transformation.[25] The ZnO nanocrystals can grow further into ZnO NWs, but their length and diameter are limited by the sizes of the initial ZnO nanocrystals, as shown for the case of room temperature growth (see Fig. 3g and h). Because of high surface energy, the ZnO NWs tend to form bunches and interconnect to form self-organized structures, which can fuse into larger and perfect ZnO NWs with increasing temperature, as shown in Figure 3. It is worth noting that the pores or gaps still exist, even though the bunches are interconnected into a continuous curst. Szpak and Gabriel[30] showed that type II ZnO can be directly created without the occurrence of type I ZnO in an environment where the OH^- concentration is low but the ZnO_2^{2-} ions remain saturated in the electrolyte. Coincidentally, such a dense type I ZnO NW crust on the Zn microsphere will effectively impede the fast diffusion of OH^- ions to the interface of metallic Zn as well as the rapid diffusion of the ZnO_2^{2-} and H_2O away from the interface. The two conditions, that is, low OH^- and saturated ZnO_2^{2-} concentration, are satisfied simultaneously. Therefore, as suggested by Szpak et al., when the type I ZnO NW shell is formed, type II ZnO continues to grow until the metallic Zn is consumed. Subsequently, ZnO_2^{2-} ions produced from ZnO with OH^- can diffuse from inside the microspheres into the solution. Because of the existence of pores as well as the nonuniformity of the ZnO NW crust, some facets with thin ZnO NW shell could fall off, leaving the ZnO microsphere crust with an open mouth. In solution, ZnO nanocrystals can nucleate and grow from $Zn(OH)_4^{2-}$ units into bunched ZnO NW arrays without voids at the center at higher temperatures.[31] The growth of the aggregates also consumes more ZnO_2^{2-} ions in solution, inducing a large concentration gradient for the ZnO_2^{2-} ions from the Zn microsphere surface to the solution which may be a dominant driving force for the diffusion of the ZnO_2^{2-} ions from the inner of the ZnO microspheres into the solution and thus the dissolution of the metallic Zn.

Another important finding that should be mentioned is that in solution ZnO nucleates and grows into large micrometer-sized, rhombus-shaped particles instead of NWs at room temperature. The result indicates that the formation of the ZnO NWs nucleated from $Zn(OH)_4^{2-}$ units in solution depends on

ADVANCED FUNCTIONAL MATERIALS

the reaction temperature. The whole formation process of the ZnO nanoarchitectures from various sources is schematically illustrated in Figure 6.

2.3. Room-Temperature Raman and Photoluminescence Properties of Ultrathin Bunched ZnO NW Arrays on Zn Microspheres

As shown above, the size of the ZnO NWs created on the Zn microspheres can be controlled by adjusting the reaction temperature. An alternative approach to the preparation of ultrathin bunched ZnO NWs on Zn microspheres is to change the reactant concentration. After doubling the quantity of Zn powder to 2.6 g and reacting with ZnO_2^{2-} ions for 12 h at room temperature, we found that a large number of ultrathin ZnO NW clusters formed on the Zn microspheres instead of ZnO NW hollow spheres, besides a few rhombus-shaped ZnO particles, as shown in Figure 7. Figure 7a and b shows low-resolution SEM images, while Figure 7c–f shows higher-magnification SEM images of the products. It can be seen that various patterns, such as squares and circles, have been formed on the surfaces of the Zn microspheres. The patterns are composed of ZnO NW arrays. Each of them contains many ultrathin ZnO NWs with an average diameter of ca. 10 nm (see Fig. 1e). The ultrathin ZnO NWs are actually formed by "gluing" together much thinner ones (ca. 5 nm). In Figure 7f, the cementing slits in the ultra-thin ZnO NWs can be clearly observed. Adjacent ultrathin ZnO NWs tend to aggregate together to form bunches

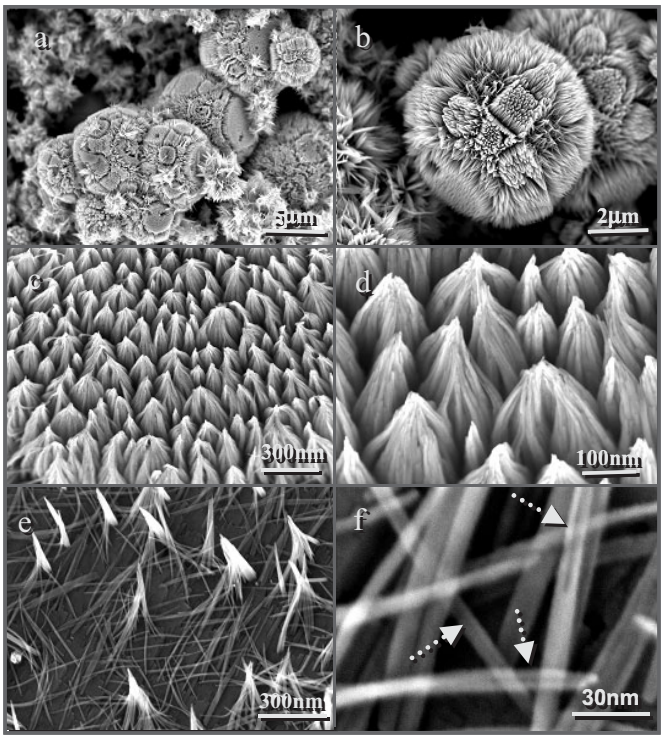

Figure 7. FE-SEM images of the ultrathin ZnO NW clusters grown on the Zn microspheres at room temperature. a,b) Low-resolution images. c–f) High-resolution images. The arrows in (f) indicate the cementing slits between thinner ZnO NWs.

The morphology and crystallographic orientation of the ZnO NWs can be further determined in detail by TEM. Although the ZnO NWs assemble into clustered aggregates, individual ZnO NW can still be found on certain surfaces of a Zn microsphere, as shown in Figure 7e and f. Figure 8 shows typical TEM images of the ZnO NWs. Figure 8a shows several individual ZnO NWs on the surface of a Zn microsphere that exhibit a straight shape and uniform diameters. From the high-resolution (HR) TEM image recorded from a segment of an individual ZnO NW (see Fig. 8b), the distance between the parallel lattice planes was been measured to be 0.28 nm, corresponding

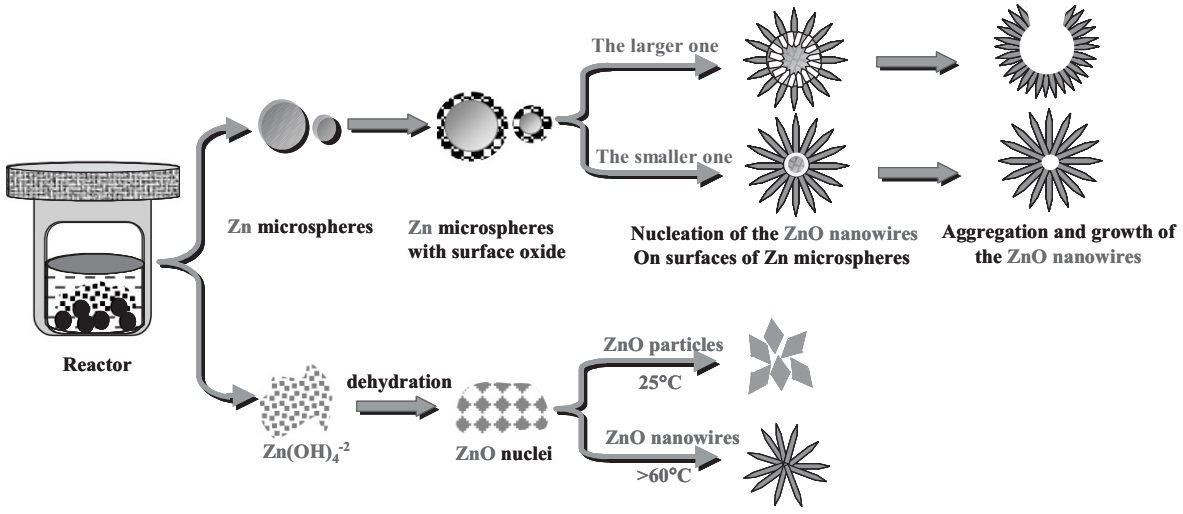

Figure 6. Schematic illustration of possible growth process of the ZnO NWs aggregates formed on metallic Zn microsphere as well as in concentrated NaOH aqueous solution with existence of the zincate ions. Noting that rhombus-shaped ZnO particles appear instead of the ZnO NWs in the solution at room temperature.

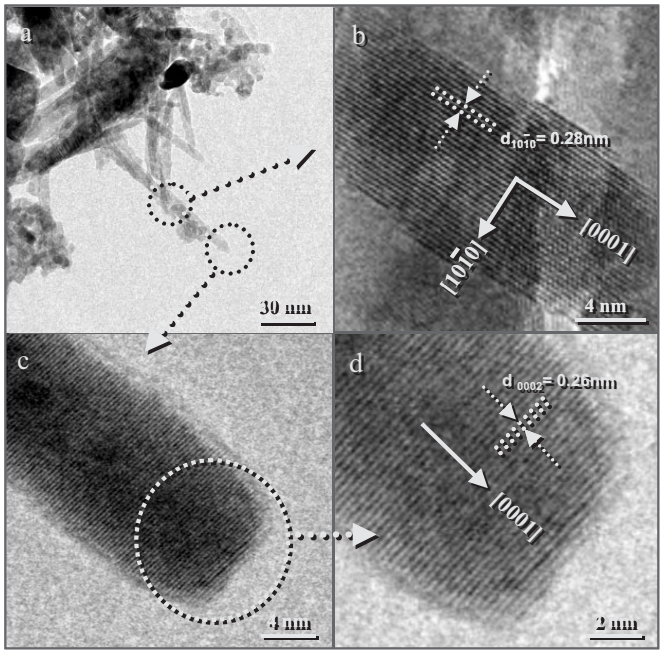

Figure 8. TEM images of ultrathin ZnO NWs grown on the Zn microspheres at room temperature. a) Low-resolution TEM morphology of the ultrathin ZnO NWs. b) HRTEM image of a segment of an individual ZnO NW. c) HRTEM image of a segment from the top of the same ZnO NW. d) Enlarged high-resolution TEM image of the ZnO NW apex.

to a *d*-spacing of the (10–10)-planes. Figure 8c and d shows HRTEM images of a segment of the top of the same ZnO NW, from which the lattice distance measured from lattice fringes along the growth axis direction of the ZnO NW is 0.26 nm, coincident with the space between (0002) planes for wurtzite ZnO. The results unambiguously confirm that the ZnO NWs have wurtzite single crystalline structure grown along the [0001] *c*-axis direction.

ZnO crystal exhibits the hexagonal wurtzite structure, which belongs to the space group C_{6V}^4. According to the selection rules of phonon resonance modes, Raman-active modes for wurtzite ZnO are $A_1 + 2E_2 + E_1$.[32] The A_1 and E_1 modes are polar and can split into the transverse optical (TO) and longitudinal optical (LO) phonon modes. The E_2 mode is nonpolar optical phonon mode that is composed of two modes with a low and a high frequency. Figure 9 demonstrates the Raman spectrum of the ultrathin ZnO NW clusters in the wavenumber range 50–800 cm^{-1} at room temperature. Vibration peaks can be clearly observed at 100, 332, 385, 440, and 581 cm^{-1}. The peaks at 385 and 581 cm^{-1} correspond to the polar transverse A1 and longitudinal E1 optical phonon mode, respectively. The two strong peaks at 100 and 440 cm^{-1} can be assigned to the two nonpolar optical phonon (E_2) modes of the ZnO NWs at low and high frequency, respectively, which are associated with oxygen deficiency. The peak at 332 cm^{-1} is attributed to the $2E_2$ mode. A strong intensity of the E_2 modes implies that the ZnO NWs grown at room temperature are severely oxygen deficient in comparison with those synthesized at high temperature, which exhibit a very low oxygen vacancy. Further analysis reveals that the full width at half maximum (FWHM) of the E_2

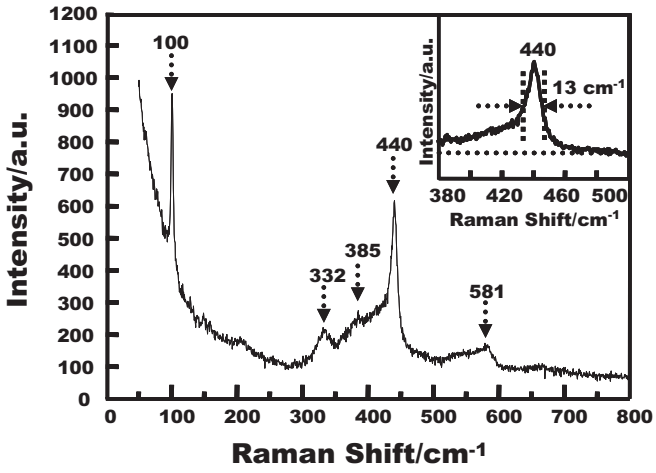

Figure 9. Raman scattering spectrum of ultrathin ZnO NW clusters grown on Zn microspheres at room temperature. The insert shows a region of the spectrum.

(440 cm^{-1}) mode is (13 ± 1) cm^{-1}. Previous studies[33,34] showed that the phonon confinement effect could induce broadening and asymmetry of the Raman peaks. When the size of ZnO nanoparticles decreases to below 21 nm, the FWHM of the Raman peak for the E_2 vibration mode rapidly broadens, reaching 11 cm^{-1} for ZnO nanoparticles of 10 nm in size.[32] In our case, the FWHM at for the E2 mode 440 cm^{-1} has been estimated as 13 cm^{-1}, which is a little larger than that of ZnO nanoparticles. We believe that oxygen deficiency and residual stress existing in the ZnO NWs could contribute to the broadening of the Raman optical phonon mode, besides the size effect.[35]

Room-temperature photoluminescence was recorded with at an excitation wavelength of 340 nm. In Figure 10, the peak around 387 nm (3.2 eV) is usually attributed to recombination of free excitons, that is, near band-edge emission. Other peaks

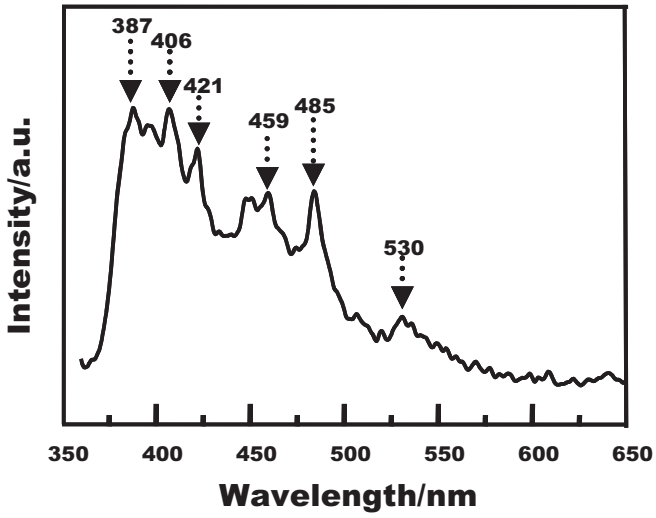

Figure 10. Room-temperature photoluminescence spectrum of ultrathin ZnO NWs grown on Zn microspheres.

ADVANCED FUNCTIONAL MATERIALS

at 406 nm (3.1 eV), 421 nm (3.0 eV), 459 nm (2.7 eV), 485 nm (2.6 eV), and 530 nm (2.3 eV) probably originate from defect-state luminescence. It is known that visible luminescence mainly originates from defect states such as Zn interstitials and oxygen vacancies. In general, oxygen vacancies can act as luminescence centers.[36] Oxygen exhibits three kinds of charge states of oxygen vacancies such as V_{O^0}, V_{O^+}, and $V_{O^{2+}}$. The oxygen vacancies are located below the bottom of the conduction band (CB) in the sequence of V_{O^0}, V_{O^+}, and $V_{O^{2+}}$, from top to bottom. The peak around 530 nm may be related to the singly ionized oxygen vacancy. The green emission results from the recombination of a photogenerated hole with a singly ionized charge state of the specific defect. Theoretical calculations on the energy levels of intrinsic point defects demonstrate that vacant Zn (Vzn) and interstitial O (Oi) produce shallow acceptor levels at 0.3 and 0.4 eV above the top of valence band (VB), and that interstitial Zn (Zni) produces a shallow donor level at 0.5 eV below the bottom of CB.[37] $V_{O^{2+}}$ produces a deep donor level at 1.3 eV below the bottom of CB. V_{O^+} lies around 2.4 eV at the bottom of CB.[38,39] Figure 11 schematically depicts the positions of the possible defect levels. From Figure 11, it seems that the emission at 421 nm can be assigned to the recombination of an electron at Zni and a hole in the VB.

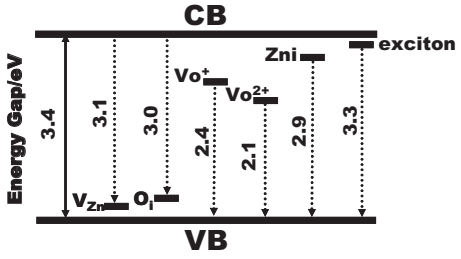

Figure 11. A schematic illustration of the intrinsic defect state levels for ZnO.

3. Conclusions

Several hierarchical structures made of bunched ZnO NW have been successfully synthesized through a wet-chemical route that uses Zn powder in a closed Teflon reactor. The formation process involves the nucleation and subsequent growth of ZnO NWs on the metallic Zn microspheres as well as in solution, in alkali condition and in the presence of zincate ions. Three different types of multidimensional bunched ZnO NW arrays have been prepared, which are believed to originate from different reaction sources. By adjusting the reaction temperature, a reasonable level of control over the sizes of the ZnO NW units on the aggregates can be achieved. At higher temperatures, such as 200 °C, ZnO NWs exhibit larger sizes with lengths of several micrometers and diameter of several hundreds of nanometers. At room temperature, ZnO NWs grown on the Zn microspheres have shorter lengths of ca. 500 nm and smaller average diameters of ca. 10 nm. Compared with various bunched ZnO arrays formed at higher temperature, double-pyramid-shaped or rhombus-shaped ZnO particles were formed at lower temperatures, besides the bunched ZnO NWs. The phenomenon may be reasonably explained by the temperature-dependent growth process of ZnO, originating from different nucleation sources. A growth mechanism has been suggested. We believe that the degree of saturation of the zincate ions in the reaction solution plays a very important role in controlling the nucleation and growth of the ZnO NWs as well as further oxidizing metallic Zn microspheres. On the basis of this consideration, ultrathin ZnO NW bunches have been successfully achieved on Zn microspheres at room temperature. The Raman spectrum and the photoluminescence behavior of the ultrathin ZnO NW clusters have also been explored.

4. Experimental

Synthesis and Purification: All reagents were analytical grade and used without further purification. For the preparation of urchin-like multidimensional ZnO nanomaterials, a typical process was as follows: Firstly, 1.3 g metallic Zn powder was added into 10 mL deionized water with continuous stirring at room temperature. Subsequently, 20 mL zincate ion (ZnO_2^{2-}) solution (0.5 M $Zn(NO_3)_2$ + 5.0 M NaOH) was mixed into the solution. The mixture was then introduced into a Teflon vessel (50 mL capacity) sealed in a stainless-steel bomb. The autoclave was heated, and maintained at the desired temperature (e.g., 200 °C) for 2 h, and then cooled to room temperature. The white product was collected and rinsed copiously with deionized water and ethanol, and was finally purified by self-sedimentation. For further characterizations, the sample was dried in vacuum.

Characterizations: The phase structures of as-synthesized products were examined by using a powder X-ray diffraction (XRD, Rigaku D/MAX2000 X-ray diffractometer with Cu Kα ($\lambda = 1.5418$ Å) radiation operating at 40 kV and 20 mA. The size, morphology, and structure of the products were observed by a scanning electron microscope (Philips XL30 S-FEG and Hitachi S-5200) and a transmission electron microscope (JEOL 2010 with an accelerating voltage of 90 kV). Samples for SEM and TEM observations were prepared by depositing the obtained products onto n-Si (100) substrates and carbon-coated copper grids, respectively. The reaction procedures under other temperature conditions were similar to those at 200 °C, except at room temperature, in which case the mixed solution was first added into a 50 ml Teflon cell with stirring for 2 h, and then the system was closed and placed without stirring at room temperature for 10 h. For the urchin-like ZnO nanomaterial synthesized at room temperature, room-temperature photoluminescence was detected by using an excitation wavelength of 340 nm with an UV-vis-near infrared (NIR) double beam spectrophotometer (Perkin Elmer, USA). μ-Raman scattering experiments were conducted by using a spectrometer (JY-T64000) with a resolution of 4 cm^{-1} in the wavenumber range from 50 to 1000 cm^{-1}. The 532 nm line of an Ar^+-ion laser served as excitation source.

Received: May 2, 2006
Revised: June 27, 2006
Published online: April 3, 2007

[1] Y. Huang, X. F. Duan, Q. Q. Wei, C. M. Lieber, *Science* **2001**, *291*, 630.
[2] M. S. Mo, J. C. Yu, L. Z. Zhang, S.-K. A. Li, *Adv. Mater.* **2005**, *17*, 756.
[3] W.-L. Lee, R.-L. Yong, *Appl. Phys. Lett.* **1996**, *69*, 526.
[4] K. G. Hendrikse, W. J. Mcgill, J. Reedijk, P. J. Nieuwenhuizen, *J. Appl. Polym. Sci.* **2000**, *78*, 2290.

[5] K. G. Hendrikse, W. J. Mcgill, *J. Appl. Polym. Sci.* **2000**, *78*, 2302.
[6] D. E. McCormack, P. O'Brien, R. Ramesh, *J. Mater. Chem.* **2003**, *13*, 2586.
[7] M. H. Huang, S. Mao, H. Feick, H. Q. Yan, Y. Y. Wu, H. Kind, E. Weber, R. Russo, P. D. Yang, *Science* **2001**, *292*, 1897.
[8] Z. L. Wang, J. H. Song, *Science* **2006**, *312*, 242.
[9] J. L. Yang, S. J. An, W. I. Park, G. C. Yi, W. Choi, *Adv. Mater.* **2004**, *16*, 1661.
[10] L. S. Wang, X. Z. Zhang, S. Q. Zhao, G. Y. Zhou, Y. L. Zhou, J. J. Qi, *Appl. Phys. Lett.* **2005**, *86*, 024 108.
[11] G. Z. Shen, Y. Bando, B. D. Liu, D. Golberg, C. J. Lee, *Adv. Funct. Mater.* **2006**, *16*, 410.
[12] B. H. Juarez, P. D. Garcia, D. Golmayo, A. Blanco, C. Lopez, *Adv. Mater.* **2005**, *17*, 2761.
[13] J. J. Wu, S. C. Liu, *Adv. Mater.* **2002**, *14*, 215.
[14] L. Vayssieres, *Adv. Mater.* **2003**, *15*, 464.
[15] B. Liu, H. C. Zeng, *J. Am. Chem. Soc.* **2003**, *125*, 4430.
[16] Q. C. Li, V. Kumar, Y. Li, H. T. Zhang, T. J. Marks, R. P. H. Chang, *Chem. Mater.* **2005**, *17*, 1001.
[17] Z. S. Hu, D. J. E. Ramírez, B. E. H. Cervera, G. Oskam, P. C. Searson, *J. Phys. Chem. B* **2005**, *109*, 11 209.
[18] M. H. Huang, Y. Wu, H. Feick, N. Tran, E. Weber, P. Yang, *Adv. Mater.* **2001**, *13*, 113.
[19] Z. W. Pan, Z. R. Dai, Z. L. Wang, *Science* **2001**, *291*, 1947.
[20] H. D. Yu, Z. P. Zhang, M. Y. Han, X. T. Hao, F. R. Zhu, *J. Am. Chem. Soc.* **2005**, *127*, 2378.
[21] X. Y. Kong, Y. Ding, R. S. Yang, Z. L. Wang, *Science* **2004**, *303*, 1348.
[22] a) X. Y. Kong, Z. L. Wang, *Nano Lett.* **2003**, *3*, 1625. b) P. X. Gao, Y. Ding, W. Mai, W. L. Hughes, C. S. Lao, Z. L. Wang, *Science* **2005**, *309*, 1700.
[23] W. Hughes, Z. L. Wang, *J. Am. Chem. Soc.* **2004**, *126*, 2709.
[24] Z. L. Wang, X. Y. Kong, J. M. Zuo, *Phys. Rev. Lett.* **2003**, *91*, 185 502.
[25] P. X. Gao, Z. L. Wang, *J. Am. Chem. Soc.* **2003**, *125*, 11 299.
[26] G. Z. Shen, Y. Bando, C.-J. Lee, *J. Phys. Chem. B* **2005**, *109*, 10 578.
[27] R. W. Powers, M. W. Breiter, *J. Electrochem. Soc.* **1969**, *116*, 719.
[28] R. W. Powers, *J. Electrochem. Soc.* **1969**, *116*, 1652.
[29] R. W. Powers, *J. Electrochem. Soc.* **1971**, *118*, 685.
[30] S. Szpak, C. J. Gabriel, *J. Electrochem. Soc.* **1979**, *126*, 1914.
[31] J. Zhang, L. D. Sun, J. L. Yin, H. L. Su, C. S. Liao, C. H. Yan, *Chem. Mater.* **2002**, *14*, 4172.
[32] T. C. Damen, S. P. S. Porto, B. Tell, *Phys. Rev.* **1966**, *142*, 570.
[33] H. Richter, Z. P. Wang, L. Ley, *Solid State Commun.* **1981**, *39*, 625.
[34] I. H. Campbell, P. M. Fauchet, *Solid State Commun.* **1986**, *58*, 739.
[35] H. T. Ng, B. Chen, J. Li, J. Han, M. Meyyappan, J. Wu, S. X. Li, E. E. Haller, *Appl. Phys. Lett.* **2003**, *82*, 2023.
[36] K. Vanheusden, C. H. Seager, W. L. Warren, D. R. Tallant, J. A. Voigt, *Appl. Phys. Lett.* **1996**, *68*, 403.
[37] P. S. Xu, Y. M. Sun, C. S. Shi, F. Q. Xu, H. B. Pan, *Nucl. Instrum. Methods Phys. Res., Sect. B* **2003**, *199*, 286.
[38] S. B. Zhang, S. H. Wei, A. Zunger, *Phys. Rev. B* **2001**, *63*, 075 205.
[39] Y. Chen, D. M. Bagnall, Z. Zhu, T. Sekiuchi, K.-T. Park, K. Hiraga, T. Yao, S. Koyama, M. Y. Shen, T. Goto, *J. Cryst. Growth* **1997**, *181*, 165.